

Research Scanning Polarimeter (RSP) cloud optical property neural network algorithm Algorithm Theoretical Basis Document (ATBD), ORACLES field campaign

Kirk Knobelspiesse¹, Daniel J. Miller¹, and Michal Segal-Rozenhaimer^{2,3,4}

¹NASA Goddard Space Flight Center, Greenbelt, MD, USA

²NASA Ames Research Center, Moffett Field, CA, USA

³Bay Area Environmental Research Institute, Moffett Field, CA, USA

⁴Geophysics Dept., Porter School for the Environment and Earth Sciences, Tel-Aviv University, Tel-Aviv, Israel

Correspondence: Kirk Knobelspiesse, kirk.knobelspiesse@nasa.gov

Table of Contents

1.	PRODUCT SUMMARY	1
2.	ALGORITHM DESCRIPTION	1
3.	IMPLEMENTATION	4
4.	ASSESSMENT	5
5.	REFERENCES	9
6.	DATA ACCESS	10

1. Product Summary

This document describes a dataset of cloud optical properties generated from the airborne Research Scanning Polarimeter (RSP) remote sensing observations during the multi-year Observations of Aerosols above Clouds and their Interactions (ORACLES) field campaign. The algorithm is based on a Neural Network (NN) that has been trained on modeled clouds as they would be observed by RSP for a variety of conditions, and is described in Miller et al. (2020). This is the second version of this product (denoted V2), an earlier version (V1) is described in Segal-Rozenhaimer et al., (2018). Note that in the file naming convention, revisions numbers start at R0, indicating that these are the first files submitted to the ESPO or ASDC archives.

This algorithm takes as input multi-angle polarimetric measurements in seven visible, near-infrared and short-wave infrared channels and produces an estimate of Cloud Optical Thickness (τ) and cloud droplet size distribution Effective Radius (r_e).

2. Algorithm Description

The algorithm is specifically designed for the RSP, an airborne scanning polarimeter with a single pixel wide swath (Cairns et al., 1999). This instrument scans in the fore and aft flight direction at to make 152 observations at View Zenith Angles (VZA) of $\pm 60^\circ$ (angular resolution

of 0.802°). To avoid vignetting and differences based on aircraft direction, this algorithm only uses observations in the $\pm 45^\circ$ range (112 angles). The RSP has nine channels with spectral band center wavelengths of 0.410, 0.470, 0.555, 0.670, 0.865, 0.960, 1.59, 1.88, 2.26, μm . Two of these channels (0.960 and 1.88 μm) are sensitive to water vapor concentration. They are thus not used directly in the NN algorithm, but they are used to determine water vapor concentration and account for its radiometric effects in other channels prior to the application of the NN. Furthermore, the RSP is sensitive to linear polarization, so inputs to the RSP are both the total reflectance (\mathbf{R}_I) and the Degree of Linear Polarization (\mathbf{DoLP}), which expresses the ratio of linearly polarized to total light. The NN algorithm thus takes 112 angles x 7 channels x 2 polarization states = 1,568 measurement as input per pixel, and produces τ and \mathbf{r}_e . The measurement inputs have variable uncertainty. Notably, \mathbf{DoLP} is generally an order of magnitude more certain than \mathbf{R}_I . Thus, a weighting scheme described in Miller et al., (2020), section 3.2 is implemented, which uses an RSP uncertainty model described in Knobelspiesse et al., (2019).

As described in more detail in Miller et al., (2020), section 3.3, this algorithm actually consists of two separate NN's, one for each product (τ and \mathbf{r}_e). While both are deep (four hidden layers, 1,024 nodes each), use batch normalization, and are optimized with Adam (Adaptive moment estimation, implemented within the Keras python API, Chollet, 2017), they use different activation functions. When comparing to other datasets, we found that the hyperbolic tangent (TANH) produced the best results for \mathbf{r}_e , while the rectified linear unit function (RELU) is best for τ . The result of these different NN's are combined into single files in the archive.

The NN's were trained with synthetic data created by a polarized doubling-adding radiative transfer model developed at the NASA Goddard Institute for Space Studies (van de Hulst and Irvine, 1963, Hansen and Travis, 1974, Cairns and Chowdhary, 2003). Because the RSP was deployed on different aircraft during ORACLES, we created different training sets for the high altitude ER-2 (used for RSP in 2016) and the lower altitude P-3 (used for RSP in 2017 and 2018). The ER-2 flies at a near constant altitude of about 20km. The P-3 flies at variable altitudes, flight segments in the 5-7km range were most ideal for RSP remote sensing.

Table 1. Parameter grid space used to generate the training set ($N = 44,064$ cases) for the operational NN used for cloud retrievals from ER-2 during ORACLES 2016 field campaign. Aircraft altitude is set as constant at 20 km.

Parameter [units]	# of grid points	Training Grid
r_e [μm]	6	5, 7.5, 10, 12.5, 15, 20
v_e [-]	6	0.01, 0.03, 0.05, 0.07, 0.1, 0.15
τ [-]	6	2.5, 5, 10, 15, 20, 30
SZA [$^\circ$]	12	10, 15, 20, 25, 30, 35, 40, 45, 50, 55, 60, 65
RAA [-]	17	0, 2, 4, 6, 8, 12, 16, 20, 24, 28, 32, 40, 50, 60, 70, 80, 90

Table 2. Parameter grid space used to generate the training set ($N = 261,144$ cases) for the operational NN used for cloud retrievals from P-3 during ORACLES 2017 field campaign.

Parameter [units]	# of grid points	Training Grid
Aircraft Altitude [m]	3	5000, 6000, 7000
r_e [μm]	6	5, 7.5, 10, 12.5, 15, 20
v_e [-]	6	0.01, 0.03, 0.05, 0.07, 0.1, 0.15
τ [-]	6	2.5, 5, 10, 15, 20, 30
SZA [$^\circ$]	13	5 to 65 in increments of 5
RAA [$^\circ$]	31	0 to 90 in increments of 3

Tables 1 and 2, from Miller et al., 2020, show the parameters of the training set. Note that cloud top altitude is not one of the modified parameters. In 2016, the cloud top altitude was relatively constant for ORACLES, and the ER-2 altitude was sufficiently high that the radiometric differences due to variable total column pressure were minimal. For 2017 and 2018, the aircraft altitude field is meant to encompass variability in not just aircraft altitude, but cloud top altitude. It is a retrieval of both.

In practice, then, there are four NN's that are used for this data product: one each for the TANH and RELU activation functions for both the [2016] and [2017,2018] training sets.

We should also note that this is not the only algorithm for the retrieval of cloud properties from RSP. The bispectral approach (Nakajima and King, 1990) uses reflected spectral ratios to determine τ and r_e , and is the basis of many satellite remote sensing algorithms. The polarimetric approach, on the other hand, uses multi-angle polarimetric observations of the cloud to determine r_e and the effective variance, v_e (τ is later determined from reflectances), (Bréon and Goloub, 1998). These algorithms are sensitive to fundamentally different phenomena, as is explored in Miller et al, (2018). RSP has the capability to make the measurements required for both of those approaches, and as such includes two different parameter results in the WTRCLD product. The NN algorithm, on the other hand, incorporates both radiometric and polarimetric data and therefore can act like either algorithm. In observations where the clouds were optical thick and spatially homogenous, this algorithm tends to act more like a polarimetric retrieval. In the more difficult cases, with optically thinner and spatially heterogenous clouds, the NN algorithm produces results more similar to the bispectral algorithm.

Finally, the effective variance, v_e , is a parameter we do not include in our archival files. While this is a parameter that was incorporated into our NN training set, and is retrieved with standard polarimetric algorithms, we found that its retrieval with the NN's was not robust.

3. Implementation

The NN algorithm has several steps, as is illustrated in Figure 1.

1. "Level 1" (radiometric and polarimetric) data are reorganized so that they represent multi-angle views of the cloud top. The assumed altitude of this reorganization is 1000m, based on parallax.
2. Standard WTRCLD files are created. Two products in these files are used in NN processing:
 - a. A liquid water cloud mask
 - b. Above cloud water vapor pressure derived from the 0.960 and 1.88 μ m channels
3. Next, level 1 observations are assessed individually. If they represent a cloud (2a) then the above cloud water vapor pressure (2b) and model reanalysis (MERRA-2 output and standard atmosphere vertical profiles) are used to correct for trace gas absorption.
4. The corrected data are then standardized (weighted) using expectations of R_I and $DoLP$ measurement uncertainty.
5. The appropriate NN ([2016] or [2017,2018]) is applied for both the RELU and TANH cases to determine τ and r_e . The results are combined into a single file, archived in both ICARTT and NetCDF formats.

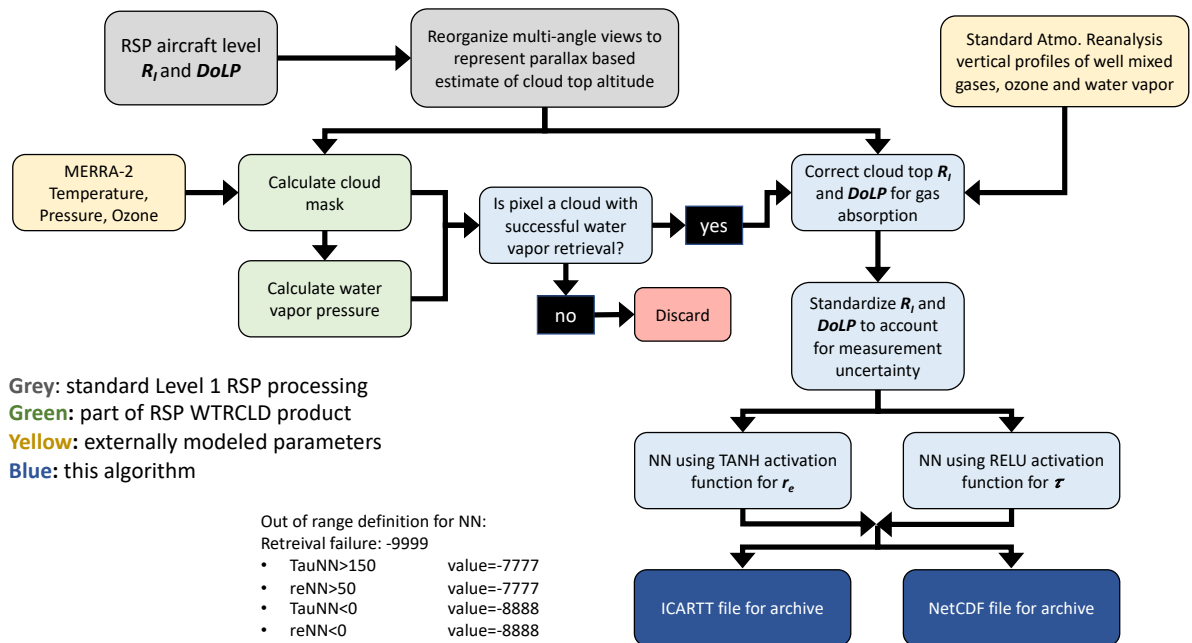


Figure 1 NN algorithm flowchart.

4. Assessment

This section provides a general assessment of the RSP NN cloud retrieval dataset, in terms of its statistical likelihood, variability from year to year, sensitivity to geometry, and comparisons to bispectral and polarimetric retrievals in the WTRCLD product. A more in-depth analysis is found in Miller et al., (2020).

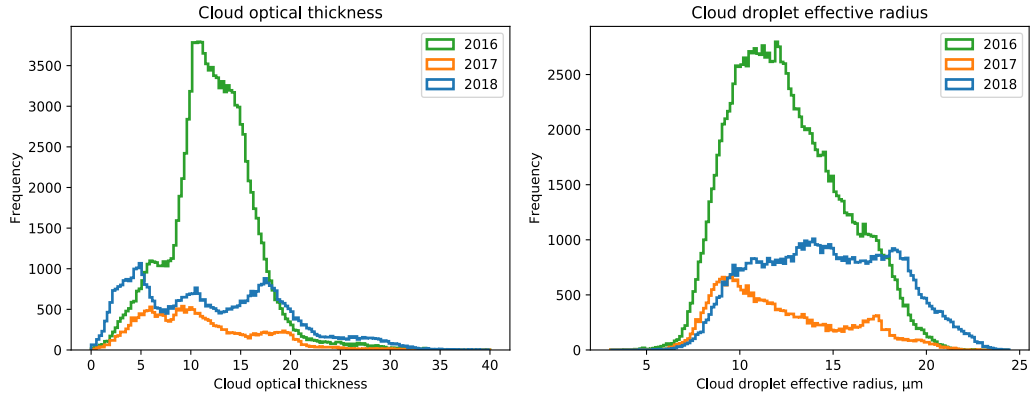


Figure 2 contains histograms for τ and r_e , broken down by year. These histograms have not been normalized, so it is clear that more observations were made in 2016 than the other years. This is because the ER-2 continuously operated in a manner appropriate for remote sensing instruments, while in other years the P-3 aircraft served the needs of both remote sensing and in situ sampling instruments. We can also see that 2016 properties were generally monomodal, and more narrowly distributed than other years.

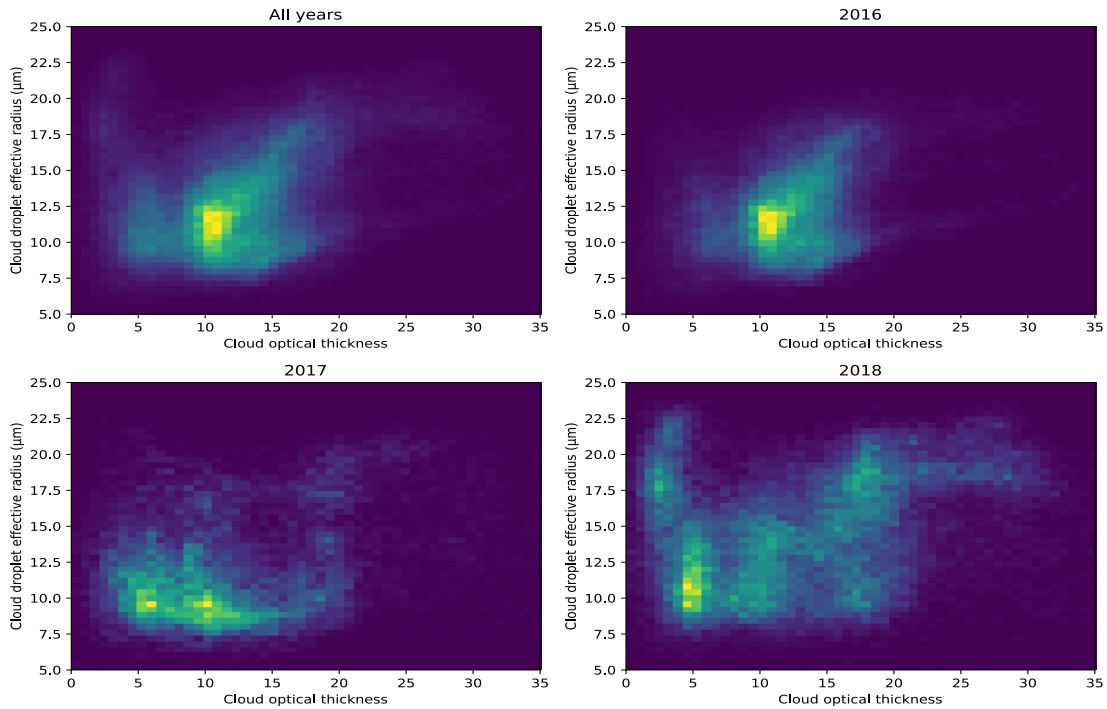


Figure 3 shows 2D histograms of τ and r_e . We can see that 2016 is dominated by a single mode with both τ and r_e around 11, with τ and r_e monotonically increasing together in a linear fashion. This is not the case for other years, which also show a mode of lower optical depth (around 5) and effective radius, but wider overall range.

Both the bispectral and polarimetric cloud retrieval algorithms can be sensitive to measurement geometry. This is especially the case for the latter, which needs to observe the cloud bow and other features that are exhibited at very specific scattering angles. We therefore assessed the sensitivity of our results to the maximum scattering angle in each observation. It is clear from Figures 4 and 5 that there is minimal sensitivity to scattering angle maximum, although we should note that the WTRCLD retrieval algorithm, used to identify the presence of clouds, is only activated for observations with at least a maximum scattering angle of 150° .

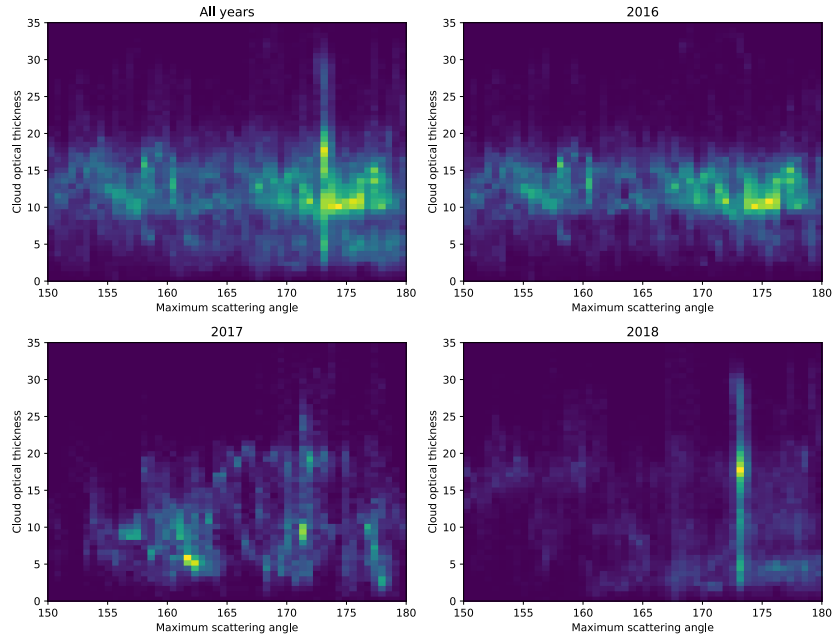


Figure 4 2D histogram of maximum scattering angle versus cloud optical thickness.

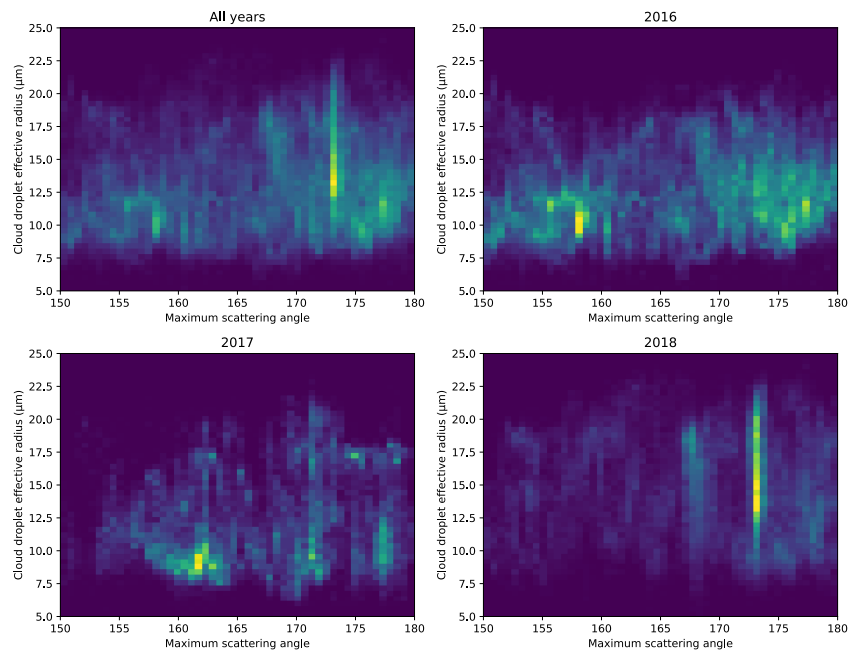


Figure 5 2D histogram of maximum scattering angle versus cloud droplet effective radius.

ORACLES 2016 - r_e

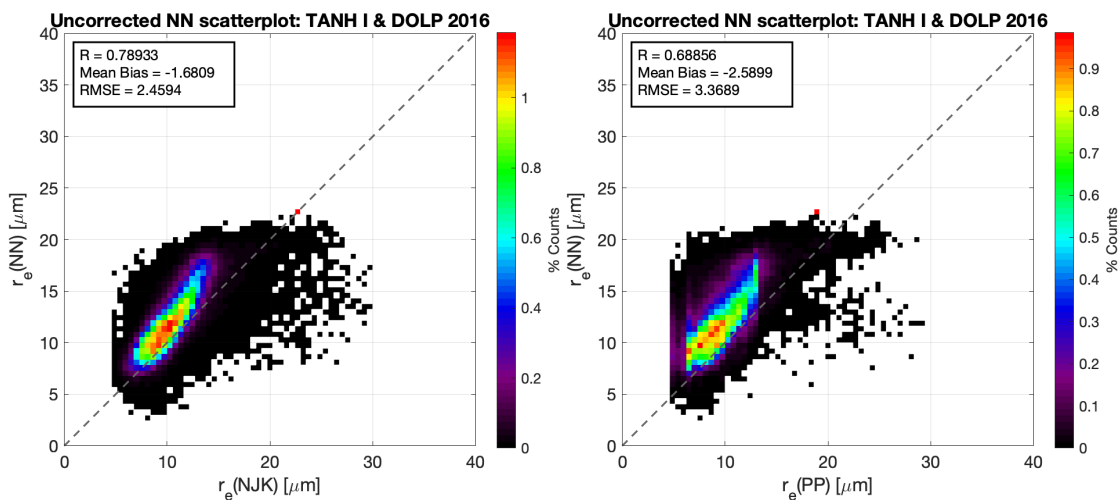


Figure 6 2016 NN effective radius retrieval with respect to bispectral (left) and polarimetric (right) algorithms.

ORACLES 2016 - τ

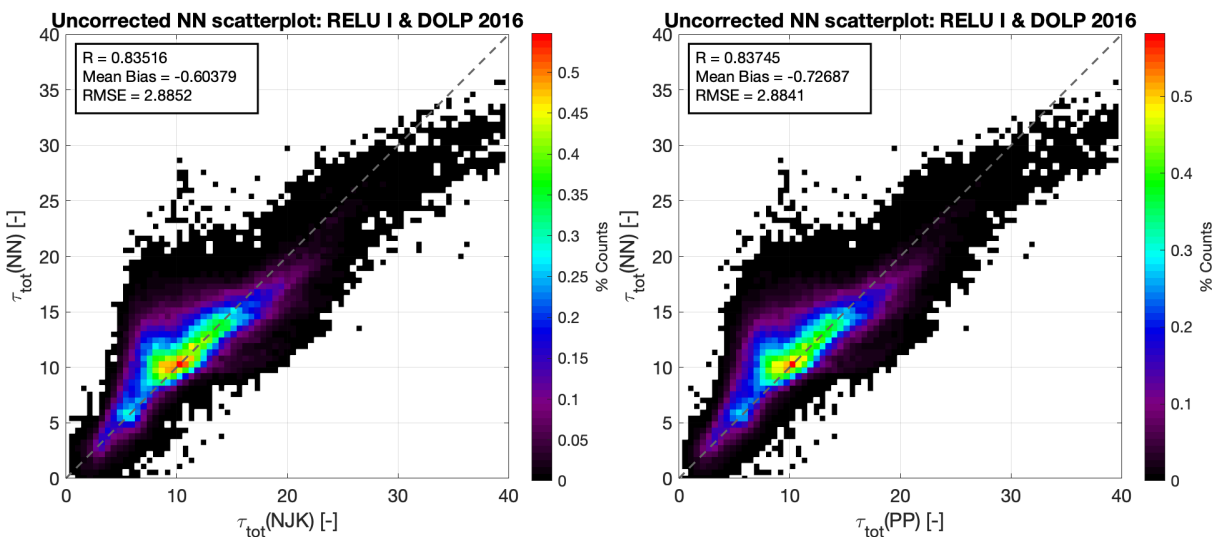


Figure 7 2016 NN cloud optical thickness with respect to bispectral (left) and polarimetric (right) algorithms.

ORACLES 2017 - r_e

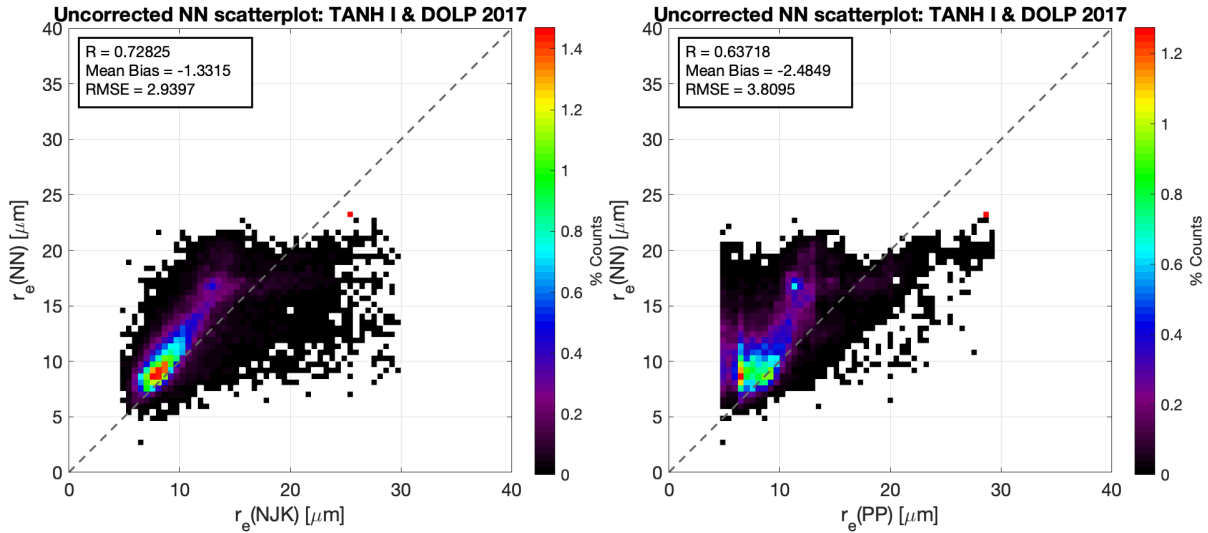


Figure 8 2017 NN effective radius retrieval with respect to bispectral (left) and polarimetric (right) algorithms.

ORACLES 2017 - τ

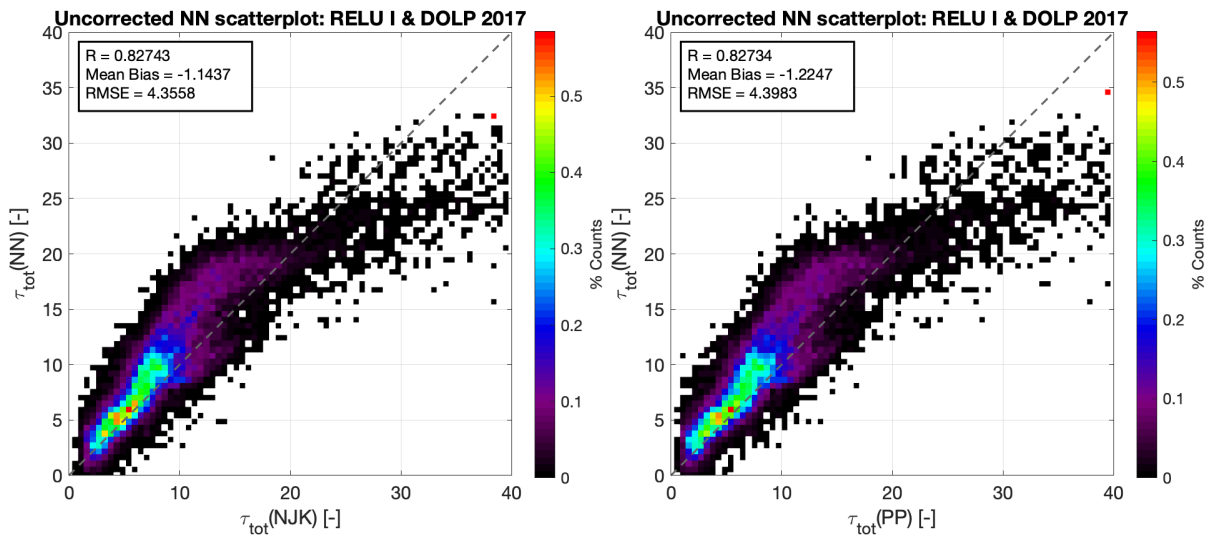


Figure 9 2017 NN cloud optical thickness with respect to bispectral (left) and polarimetric (right) algorithms.

ORACLES 2018 - r_e

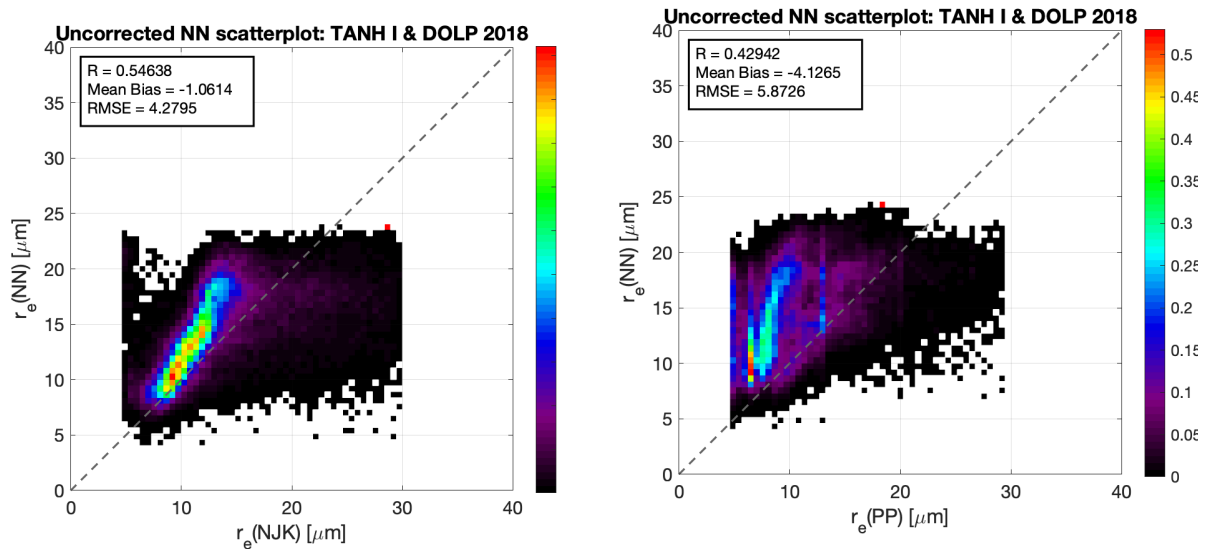


Figure 10 2018 NN effective radius retrieval with respect to bispectral (left) and polarimetric (right) algorithms.

ORACLES 2018 - τ

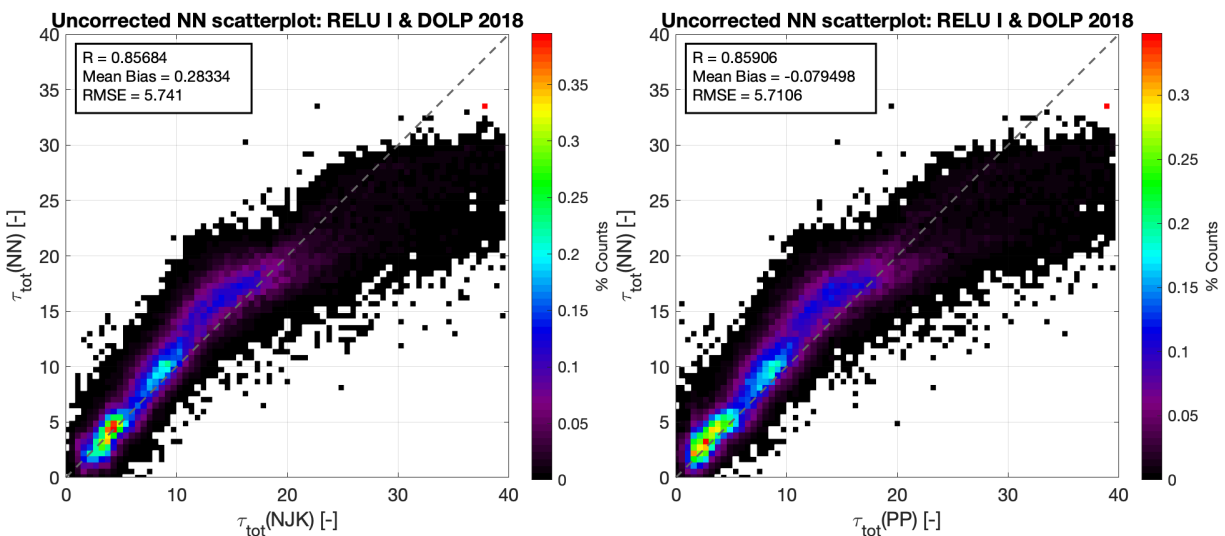


Figure 11 2018 NN cloud optical thickness with respect to bispectral (left) and polarimetric (right) algorithms.

5. References

Bréon, F.M. and Goloub, P., 1998. Cloud droplet effective radius from spaceborne polarization measurements. *Geophysical research letters*, 25(11), pp.1879-1882.

- Cairns, B. E.E. Russell, and L.D. Travis, 1999. Research Scanning Polarimeter: calibration and ground-based measurements, *Proc. SPIE 3754, Polarization: Measurement, Analysis, and Remote Sensing II, (25 October 1999)*; <https://doi.org/10.1117/12.366329>
- Cairns, B. and Chowdhary, J. 2003. Aerosol Polarimetry Sensor Algorithm Theoretic Basis Document, Tech. rep., available: https://glory.giss.nasa.gov/aps/docs/APS_ATBD.pdf
- Chollet, F. 2017. Deep Learning with Python , *Manning Publications Co.*, Greenwich, CT, USA, 1st edn.
- Hansen, J. E. and Travis, L. D. 1974. Light scattering in planetary atmospheres, *Space Science Reviews*, 16, 527–610.
- Knobelspiesse, K., Tan, Q., Bruegge, C., Cairns, B., Chowdhary, J., van Diedenhoven, B., Diner, D., Ferrare, R., van Harten, G., Jovanovic, V., Ottaviani, M., Redemann, J., Seidel, F., and Sinclair, K. 2019. Intercomparison of airborne multi-angle polarimeter observations from the Polarimeter Definition Experiment, *Applied Optics*, 58, 650–669, DOI: 10.1364/ao.58.000650
- Miller, D. J., Zhang, Z., Platnick, S., Ackerman, A. S., Werner, F., Cornet, C., and Knobelspiesse, K. 2018. Comparisons of bispectral and polarimetric retrievals of marine boundary layer cloud microphysics: case studies using a LES–satellite retrieval simulator, *Atmos. Meas. Tech.*, 11, 3689–3715, <https://doi.org/10.5194/amt-11-3689-2018>.
- Miller, D. J., Segal-Rozenhaimer, M., Knobelspiesse, K., Redemann, J., Cairns, B., Alexandrov, M., van Diedenhoven, B., and Wasilewski, A. 2019. Low-level liquid cloud properties during ORACLES retrieved using airborne polarimetric measurements and a neural network algorithm, *Atmos. Meas. Tech. Discuss.*, <https://doi.org/10.5194/amt-2019-327>, in review, 2019.
- Nakajima, T. and King, M. D. 1990. Determination of the optical thickness and effective particle radius of clouds from reflected solar radiation measurements. Part I: Theory, *J. Atmos. Sci.*, 47, 1878– 1893.
- Segal-Rozenhaimer, M., D. J. Miller, K. Knobelspiesse, J. Redemann, B. Cairns, and M. D. Alexandrov. 2018. Development of neural network retrievals of liquid cloud properties from multi-angle polarimetric observations. *Journal of Quantitative Spectroscopy and Radiative Transfer*, 220: 39-51, DOI: 10.1016/j.jqsrt.2018.08.030.
- van de Hulst, H. and Irvine, W. M. 1963. General Report on Radiation Transfer in Planets Scattering in Model Planetary Atmospheres, *Liege International Astrophysical Colloquia*, 11, 78–98.

6. Data Access

Data are hosted at the NASA Earth Science Projects Office (ESPO) archive separately for each year. They are additionally mirrored at the NASA GISS RSP archive. Ultimately, the ESPO archive will be migrated to the NASA Langley ASDC, to which the DOI will then point. Details are below:

2016

ESPO DOI: 10.5067/Suborbital/ORACLES/ER2/2016_V2

GISS URL: https://data.giss.nasa.gov/pub/rsp/ORACLES_2016/

2017

ESPO DOI: 10.5067/Suborbital/ORACLES/P3/2017_V2

GISS URL: https://data.giss.nasa.gov/pub/rsp/ORACLES_2017/

2018

ESPO DOI: [10.5067/Suborbital/ORACLES/P3/2018_V2](https://doi.org/10.5067/Suborbital/ORACLES/P3/2018_V2)

GISS URL: https://data.giss.nasa.gov/pub/rsp/ORACLES_2018/